

JOINT INSTITUTE
FOR NUCLEAR RESEARCH

Determination of masses of superheavy elements in the experiments on synthesis of Cn and Fl using the reactions $48\text{Ca} + 242\text{Pu}$ and $48\text{Ca} + 244\text{Pu}$.

Name: Karim Hesham

Institute: Cairo University, Faculty of Science, Physics department

Supervisor: Viacheslav Vedeneev. Flerov laboratory of Nuclear Reactions, Dubna, Russia.

• Table of contents

Abstract	2
1- Introduction	3
2- MASHA Setup	4
2.1 Ion Source.....	4
2.2 A target Assembly and Hot catcher.....	5
2.3 Detection and Control System.....	6
2.4 Experimental Method.....	7
3- Results and Discussion	8
3.1 $^{40}\text{Ar} + ^{148}\text{Sm} \rightarrow ^{188-xn}\text{Hg} + xn$	8
3.2 $^{40}\text{Ar} + ^{166}\text{Er} \rightarrow ^{206-xn}\text{Rn} + xn$	12
3.3 Multinucleon reaction of $^{48}\text{Ca} + ^{242}\text{Pu}$	15
4- Conclusions	
5- Acknowledgments	
6- References	

Abstract

The Mass Analyzer of Super Heavy Atoms or simply MASHA, is a device used to separate Atoms according to their masses, which in turn lead to their identification. It is used mainly in the production and identification of Super Heavy Elements (SHE) by their mass to charge ratio. Usage of the well known (ISOL) method to measure the masses of the produced nuclei online has been done as it is necessary for the measurement of short-lived isotopes like Hg. In the present work, mass measurement and determination of isotopes of Hg have been performed, as it is a homologue to the SHEs Cn and Fl. This may open the doors to new SHEs which are relatively stable and evidence to the existence of the so-called “Island of Stability”.

1- Introduction

Interest in the SHEs hasn't diminished since it started in the forties, where more than 20 new nuclei have been discovered since then, while in the last two decades already 5 nuclei have been discovered (${}_{113}\text{Nh}$, ${}_{115}\text{Mc}$, ${}_{116}\text{Lv}$, ${}_{117}\text{Ts}$ and ${}_{118}\text{Og}$) and research is still ongoing. These SHEs have been usually produced by the fusion reaction of ${}^{48}\text{Ca}$ and elements in the actinide series of the periodic table, the choice of ${}^{48}\text{Ca}$ is due to the fact that it is a doubly magic nucleus with proton and neutron shell closures at 20 and 28 respectively. Since the half-lives of these isotopes are really small, which is in the range of micro seconds, investigation of nuclei homologue to them like Hg is done to determine their properties. The MASHA is used to perform the synthesis of these nuclei and further determination of their properties (like the α -decay energy) from the data acquired at the position sensitive silicon detectors. The classic mass-spectrometric techniques are used for the separation and determination of the isotopes produced.

2-MASHA Setup

The structure of the MASHA is shown in Figure 1. It is composed of a hot catcher, Ion source which works on the principle of electron cyclotron resonance (ECR), then a magneto optical analyser is found which is made of four dipole lenses (D1, D2, D3a, D3b), three quadrupole lenses (Q1, Q2, Q3) and two sextupole lenses (S1, S2), and a detection system located in the focal plane of the spectrometer. The ion-optical scheme of the mass spectrometer was considered extensively in [3,4]. In this section, we describe the abovementioned separate components of the setup and present results of measurements of the essential separator characteristics.

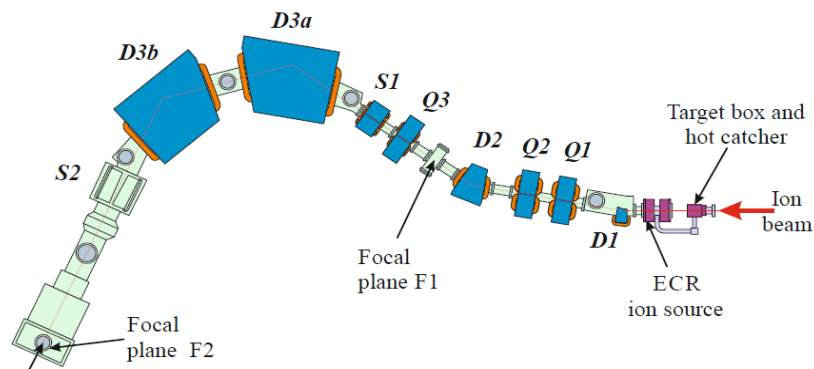


Figure 1. Schematic diagram of the MASHA mass separator: (D1, D2, D3a), and D3b) dipole magnets, (Q1, Q2, Q3) quadrupole lenses, and (S1, S2) sextupole lenses. The detection system is in the focal plane F of the separator.

2.1 Ion Source

The frequencies at which the Ion source operates are very high, in the range of 2.45 GHz. Ionization of the atoms coming from the nuclear fusion reaction occurs, where they are ionized to the charge state $Q = +1$ and accelerated up to 38 keV by a three-electrode electrostatic lens. The ion beam formed is separated by the magneto-optical mass-to-charge ratio analyser after. Obtained for noble gases, the ionization efficiency is about 90 %. Optimization of the ECR ion source occurs by using noble gases like Xenon and Krypton because of their first ionization potentials have maximum values (VIII group of the periodic table) and these are chemical inert elements (hence the name “Noble”). In this case, the operating modes of the ECR source were optimized by selecting the power and the frequency of microwave radiation and the buffer gas pressure in the

ionizer chamber. The buffer gas used was Helium, and a piezoelectric valve was used for regulation and control of pressure. At the pressure in the range of $(1-2) \times 10^{-5}$ mbar and a microwave oscillator power of ~ 30 W, the best parameters were obtained. A schematic representation of the ECR source with the hot catcher target is shown in Figure 2.

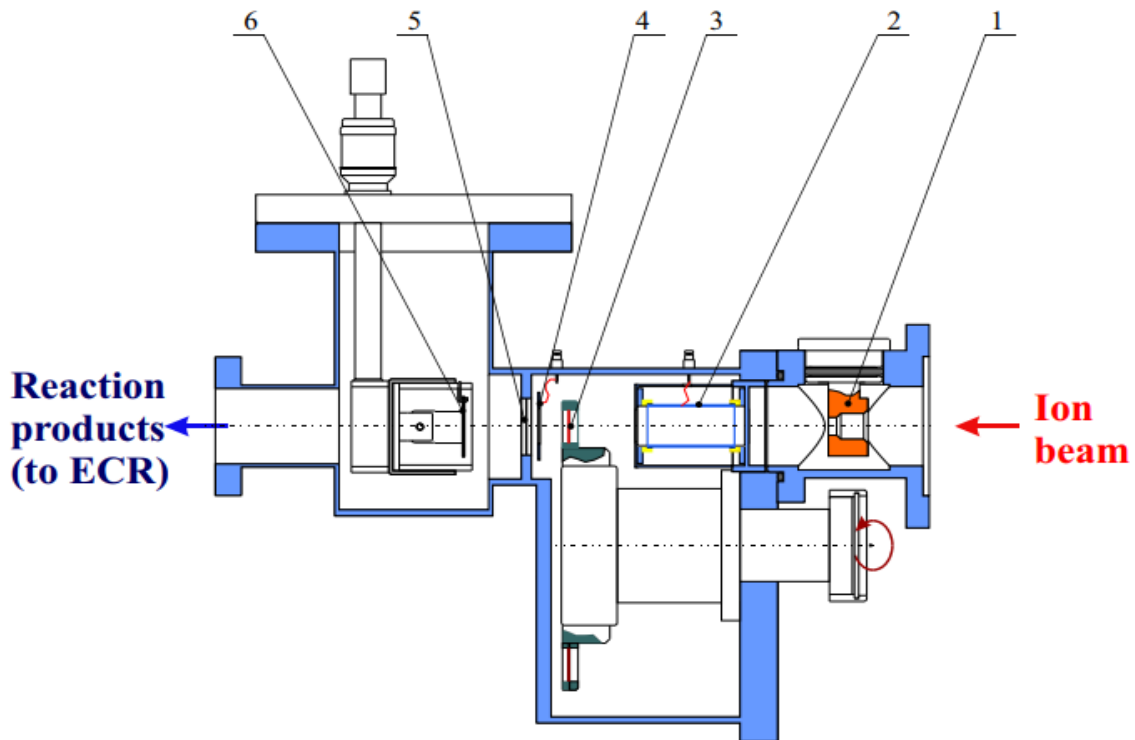


Figure 2. Schematic overview of the target-hot catcher system. Here: 1 – diaphragm; 2 – pick-up sensor; 3 – target on the wheel; 4 – electron emission beam monitor; 5 – separating foil; 6 – hot catcher.

2.2 Hot catcher and Target Assembly

The Product of the fusion reactions is a compound nucleus, this compound nucleus must be “captured”, which is done by using a hot catcher which is part of the Target. A full scheme of the hot catcher and target is shown in Figure 3. Before hitting the target, the beam of ions passes through a diagnostic system whose components are a split aperture, electrostatic induction sensor and a Faraday cup. The split aperture is divided into four sectors, each of them measures the fraction of the current beam which does not pass through the hole of the aperture. Monitoring of the current during the experiment is done by the induction sensor, which basically is a stainless-steel tube which has been placed on an

electrically isolated frame behind the split aperture. A Faraday cup is placed further behind at 70mm in front of the target placed on a rotational vacuum tight feedthrough. After the fusion reaction occurs after the interaction of the beam with the target, the products of the reaction go out of the target and enter a separating foil, where they are later trapped in a graphite absorber which is heated to temperatures of 1500 to 2000 K. Then the products diffuse as atoms and go through the pipeline into the vacuum of the hot catcher. Inside the hot catcher, there is a material which is made of heated graphite foil which has a density of 1g/cm^3 and has a thickness of 0.6mm. A disc of diameter 30mm is placed behind the target which is made of a graphite absorber, A rotating target is used so that heat can be distributed uniformly and prevent damaging of the target. The IR pyrometer is the device used to calibrate the temperature of the graphite absorber. The pyrometer could detect the radiation coming from the heated graphite. The temperature of the graphite absorber was measured during the heater current measurements, as the pyrometer could not monitor the temperature during the experiments themselves due to the arrangement of the target assembly

2.3 Detection and Control System

For the detection of nuclear reaction products, there are a wide variety of detectors like gas filled tubes (e.g., Geiger Muller) or Scintillator detector and also the newest of these detectors is semi-conductor detectors. In this work, a well know type of silicon semiconductor detector is used, which is placed in the focal plane of the mass spectrometer. The Frontal detector component is made up of 192 strips positioned perpendicular to the direction of the beam, which form the frontal sector of the detector. The detector is composed of side detectors which are divided into 16 and 64 strips. Figure 4. Shows a scheme of the detector. Typically, these detectors have an operating bias of 40V and 30keV of energy resolution for particles from a ^{226}Ra source. The assembly of the detector is configured such that at least 90% of the particles produced in the nuclear reaction is detected in the frontal section of the detector. The signals coming from each strip of the detector is read out separately. The application use shows two types of spectra, one dimensional spectrum for each strip and a two-dimensional spectrum for each crystal's energy dependency on strip number.

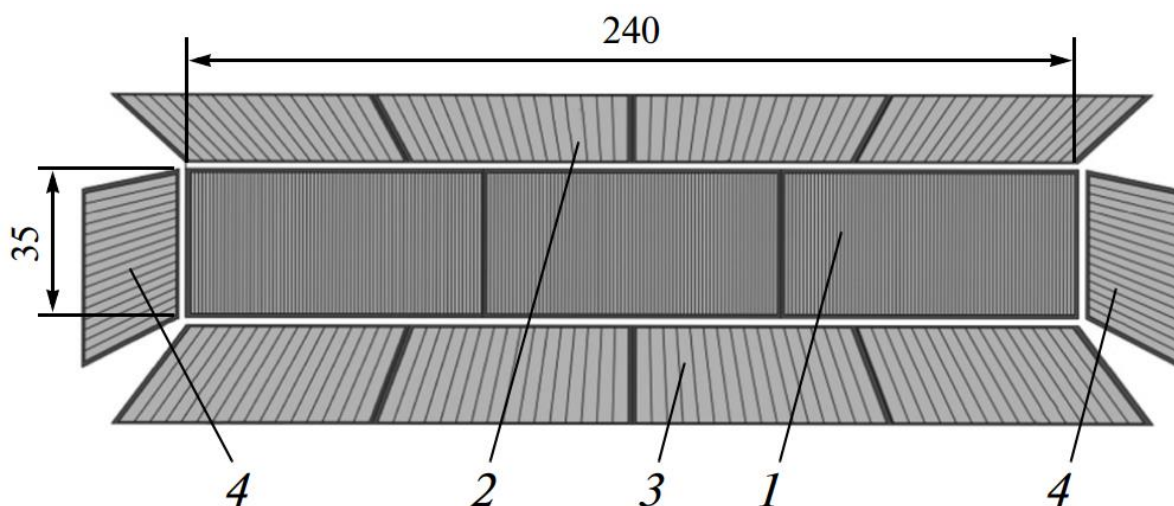


Figure 4. Frontal part (192 strips), (2) top part (64 strips), (3) bottom part (64 strips), and (4) side parts (16 strips in each).

3-Experimental Method

The ion beam is formed of ^{48}Ca Nuclei (as it is a doubly magic nucleus as mentioned which makes it more stable.) which hits the target with an energy of circa 7.3 MeV/n. The whole MASHA setup is located at one of the outlets of the U- 400M cyclotron, in which acceleration of the beam occurs to increase the cross section of the reaction as much as possible. The beam later on falls into the graphite absorber where it is stopped. We mentioned the that the target assembly consists of a hot catcher, electrostatic induction sensor and a faraday cup, which de facto controls the intensity of the beam. In these experiments as mentioned we detect Hg isotopes as it is considered a homologue to the SHEs Cn and Fl having a proton number of 112 and 114 respectively. Energies of the decay reactions were measured and compared to their theoretical values.

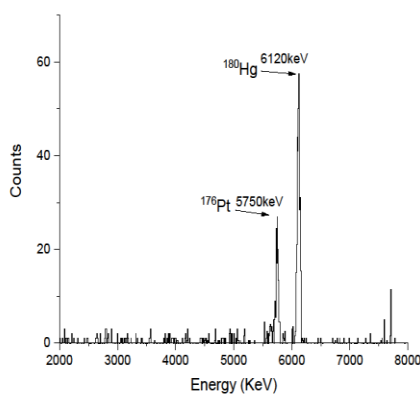
4-Results and Discussion

Analysis of the three reactions ($^{40}\text{Ar} + ^{148}\text{Sm}$, $^{40}\text{Ar} + ^{166}\text{Er}$ and $^{48}\text{Ca} + ^{242}\text{Pu}$), where the spectrum of the different isotopes is plotted and further analysed, also heatmaps for the different reactions have been done to visually results.

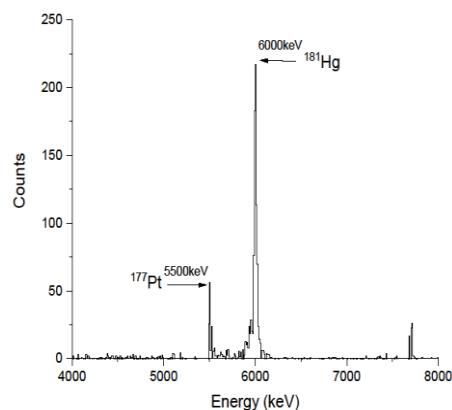


This reaction leads to the production of six isotopes of mercury (^{180}Hg , ^{181}Hg , ^{182}Hg , ^{183}Hg , ^{184}Hg and ^{185}Hg) from which we deduce that the “x” in the

reaction formula takes values from 3 to 8, implying that 3 to 8 neutrons “evaporate” during the reaction. These isotopes have been detected through their spectra via their energy releases. Figure 5. Shows the spectra for the different isotopes with their respective peaks in energy. We see that there are peaks at different lower energies than the Hg peaks which come from the energy released due to alpha decay of the Hg nucleus and the production of a daughter nucleus which is a platinum isotope, this is clear in Figure 5, (a, b and d). Comparison between the theoretical and experimental values of energy is shown in Table 1.

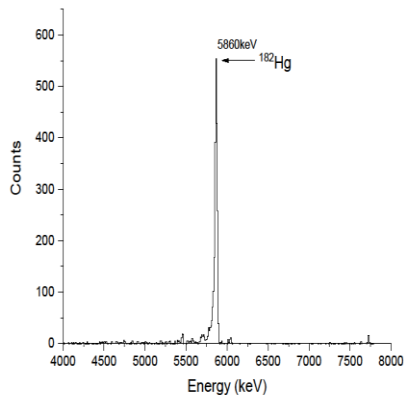


(a)

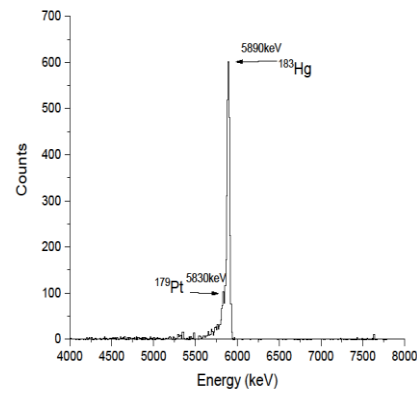


(b)

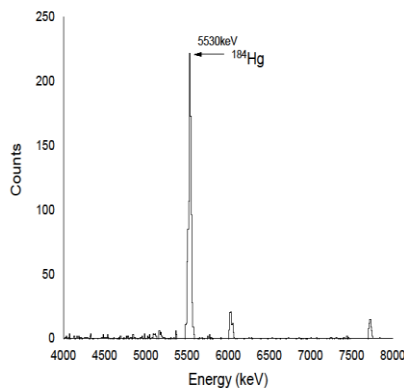
We see that in figure 5a and 5b that the peaks occur at 6120keV and at 6000keV which represent the energies released of ^{180}Hg and ^{181}Hg also smaller peaks occur as mentioned which represent the energy released by the alpha decay products of ^{180}Hg and ^{181}Hg which are ^{176}Pt and ^{177}Pt .



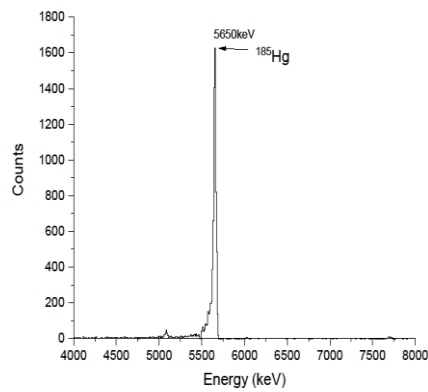
(c)



(d)



(e)



(f)

For ^{182}Hg , ^{183}Hg , ^{184}Hg and ^{185}Hg the peaks occur at 6120keV, 5890keV, 5530 keV and 5650 keV respectively. We see that in almost all graphs a recurrent peak occurs at energy circa 7700keV which, however could not be identified, it may be due to some signal noise, hence it can be treated as a systematic error. The Branching Ratios (BR) for the different isotopes are the following:

^{176}Pt (ec or $\beta^+ \rightarrow 60\%$, $\alpha \rightarrow 40\%$)

^{177}Pt (ec or $\beta^+ \rightarrow 94.3\%$, $\alpha \rightarrow 5.7\%$)

^{179}Pt (ec or $\beta^+ \rightarrow 99.76\%$, $\alpha \rightarrow 0.24\%$)

^{180}Hg (ec or $\beta^+ \rightarrow 52\%$, $\alpha \rightarrow 48\%$)

^{181}Hg (ec or $\beta \rightarrow 73\%$, $\alpha \rightarrow 27\%$)

^{182}Hg (ec or $\beta \rightarrow 86.2\%$, $\alpha \rightarrow 13.8\%$)

^{183}Hg (ec or $\beta\rightarrow 88.3\%$, $\alpha\rightarrow 11.7\%$)

^{184}Hg (ec or $\beta\rightarrow 98.89\%$, $\alpha\rightarrow 1.11\%$)

^{185}Hg (ec or $\beta\rightarrow 94\%$, $\alpha\rightarrow 6\%$)

Table 1. Comparison between the theoretical and experimental values of the energies for reaction between ^{40}Ar and ^{148}Sm .

Isotope	$T_{1/2}(\text{s})$	Energy Exp.(keV)	Energy Theo.(keV)	Percentage error
^{176}Pt	6.33	5750	5884	2.27%
^{177}Pt	10	5500	5642	2.51%
^{179}Pt	21.2	5830	5814	0.28%
^{180}Hg	2.59	6120	6258	2.20%
^{181}Hg	3.6	6000	6284	4.51%
^{182}Hg	10.83	5860	5996	2.26%
^{183}Hg	9.4	5890	6039	2.46%
^{184}Hg	30.87	5530	5660	2.29%
^{185}Hg	49.1	5650	5773	2.18%

Considering how small the error is as shown in Table 1., We can see how close are the experimental and theoretical values are to each other.

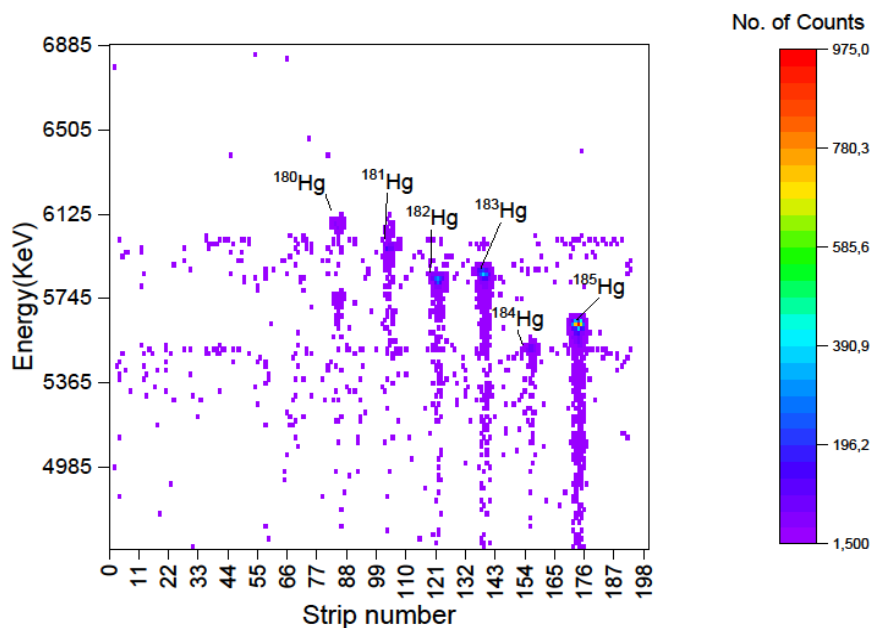
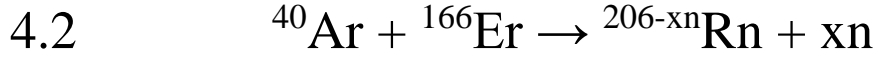
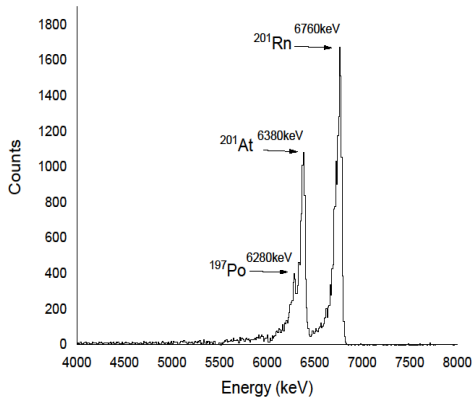


Figure 5. Heatmap for ^{40}Ar and ^{148}Sm reaction.

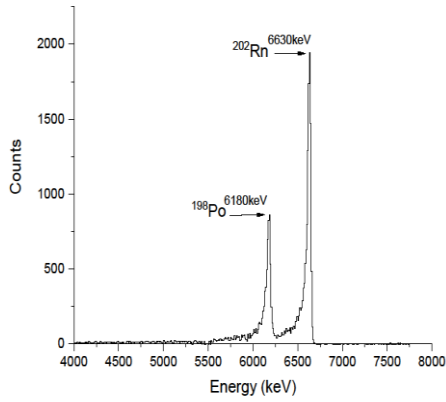
A heatmap of the reaction is shown in Figure 5. to visualize the results better.



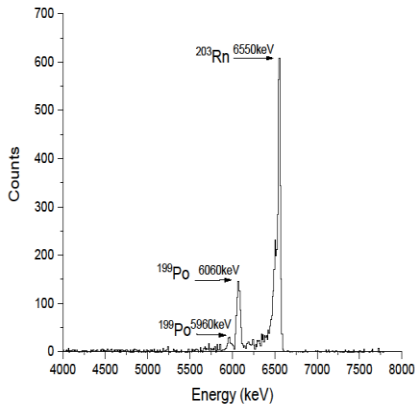
This reaction leads to the production of five isotopes of Radon which are ^{201}Rn , ^{202}Rn , ^{203}Rn , ^{204}Rn and ^{205}Rn . We deduce from this that “x” in the reaction takes values from 1 to 5. In Figure 6. We show the spectra for the different isotopes of Radon, we notice small peaks for all the reactions, these peaks represent the energy released by Polonium (Po) which is in itself a product from the alpha decay of Radon. We also notice for ^{201}Rn another peak which represents an Astatine isotope produced by beta decay of Radon.



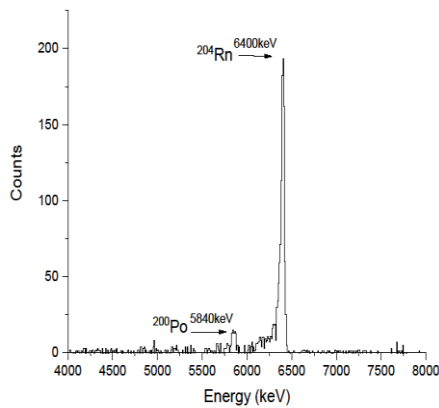
(a)



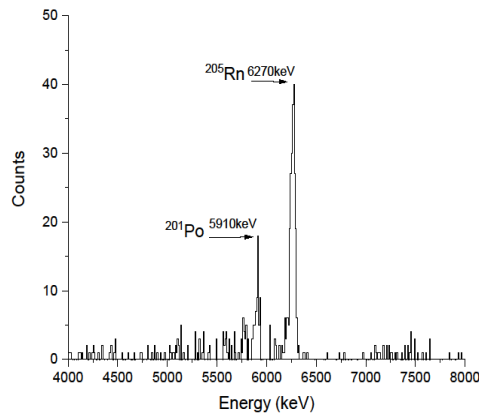
(b)



(c)



(d)



(e)

Figure 6. a) ^{201}Rn . b) ^{202}Rn . c) ^{203}Rn . d) ^{204}Rn .
e) ^{205}Rn

We see from the graphs that the peaks for ^{201}Rn , ^{202}Rn , ^{203}Rn , ^{204}Rn and ^{205}Rn are 6760keV, 6630keV, 6550keV, 6400keV and 6270keV respectively. We notice in Table 2. that the difference between the theoretical and experimental values of energies are small, from which we can deduce the high accuracy displayed by the MASHA.

Table 2. Comparison between theoretical and experimental values of energies for ^{40}Ar and ^{166}Er reaction

Isotopes	$T_{1/2}(\text{s})$	Energy Exp.(keV)	Energy Theo.(keV)	percentage error
^{197}Po	84	6280	6411	2.04%
^{198}Po	105.6	6180	6309	2.04%
^{199}Po	328	6060	6074	0.23%
^{200}Po	691	5840	5981	2.35%
^{201}Po	936	5910	5799	1.91%
^{201}At	85.2	6380	6472	1.42%
^{201}Rn	0.002	6760	6860	1.45%
^{202}Rn	0.016	6630	6773	2.15%
^{203}Rn	0.031	6550	6630	1.20%
^{204}Rn	0.057	6400	6546	2.23%
^{205}Rn	0.21	6270	6386	1.81%

The Branching Ratios (BR) for the following isotopes are:

^{197}Po (ec or $\beta^+ \rightarrow 56\%$, $\alpha \rightarrow 44\%$)

^{198}Po (ec or $\beta^+ \rightarrow 57\%$, $\alpha \rightarrow 43\%$)

- ^{199}Po (ec or β^+ \rightarrow 92.5%, α \rightarrow 7.5%)
- ^{200}Po (ec or β^+ \rightarrow 88.9%, α \rightarrow 11.1%)
- ^{201}Po (ec or β^+ \rightarrow 98.87%, α \rightarrow 1.13%)
- ^{201}At (ec or β^+ \rightarrow 29%, α \rightarrow 71%)
- ^{201}Rn (ec or β^+ \rightarrow ?, α \rightarrow ?)
- ^{202}Rn (ec or β^+ \rightarrow 22%, α \rightarrow 78%)
- ^{203}Rn (ec or β^+ \rightarrow 34%, α \rightarrow 66%)
- ^{204}Rn (ec or β^+ \rightarrow 27.6%, α \rightarrow 72.4%)
- ^{205}Rn (ec or β^+ \rightarrow 75.4%, α \rightarrow 24.6%)

As done for ^{40}Ar and ^{148}Sm reaction, a heatmap is drawn to better illustrate the data for this reaction as shown in Figure 7.

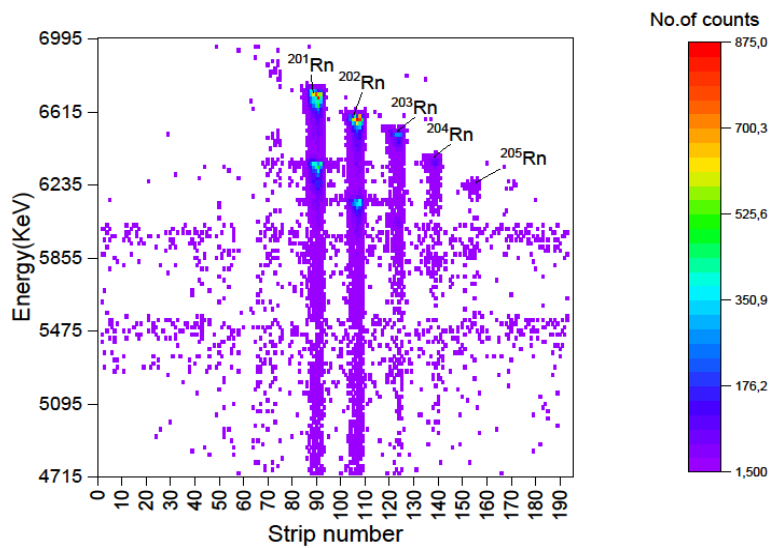
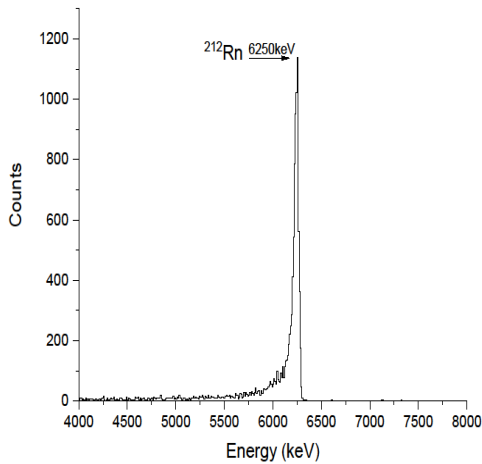


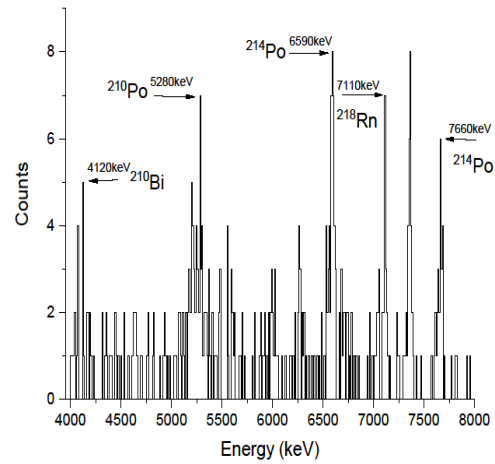
Figure.7. Heatmap of ^{40}Ar and ^{166}Er reaction

4.3 Multinucleon reaction of $^{48}\text{Ca} + ^{242}\text{Pu}$

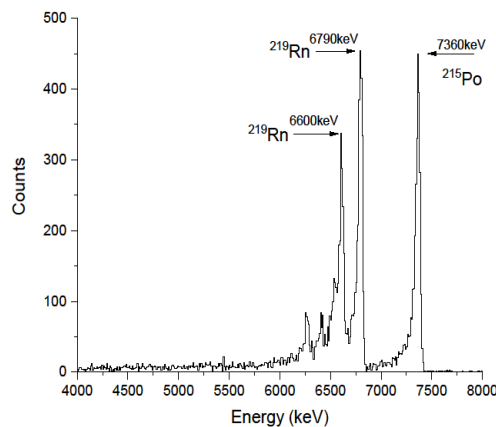
This reaction leads to the formation of different isotopes of Flerovium ($Z = 114$), which decays giving different Radon isotopes, which are detected. In Figure 8. We notice immediately the sharpness of the peaks and the easiness of their identification; this may be due to the high counting rate observed (for ^{212}Rn and ^{219}Rn) compared to the earlier reactions.



(a)



(b)



(c)

Figure 8. a) ^{212}Rn . b) ^{218}Rn . c) ^{218}Rn .

The peak energies of the three Radon isotopes are 6250keV, 7110 keV and for ^{219}Rn , two peaks are found at 6000keV and 6790keV. Polonium and Bismuth peaks also are present due to alpha decay of Radon isotopes and subsequent β^+ or ec of Polonium leading to the production of Bismuth. A possible reason for the high counting rate of ^{218}Rn could be due to its short life time, which can be seen in Table 3.

Table 3. Comparison between theoretical and experimental values of energies for ^{48}Ca and ^{242}Pu reaction.

Isotopes	$T_{1/2}(\text{s})$	Energy Exp.(keV)	Energy Theo.(keV)	Percentage error
^{210}Bi	442368	4120	4100	0.48%
^{210}Po	11955686	5280	5407	2.34%
^{212}Rn	1434	6250	6385	2.11%
^{214}Po	0.00016346	7660	7833	2.20%
^{215}Po	0.001781	7360	7526	2.20%
^{218}Rn	0.03375	7110	7262	2.10%
^{219}Rn	3.96	6790	6946	2.24%

We notice that also in this reaction, the error is small all in the range of 0% to 2.5%. The Branching Ratios for these isotopes are the following:

^{210}Bi ($\beta^- \rightarrow 100\%$, $\alpha \rightarrow 13.2\text{E-}5\%$)

^{210}Po (ec or $\beta^+ \rightarrow 0\%$, $\alpha \rightarrow 100\%$)

^{212}Rn (ec or $\beta^+ \rightarrow 0\%$, $\alpha \rightarrow 100\%$)

^{214}Po (ec or $\beta^+ \rightarrow 0\%$, $\alpha \rightarrow 100\%$)

^{215}Po ($\beta^- \rightarrow 2.3\text{E-}4\%$, $\alpha \rightarrow 99.99977\%$)

^{218}Rn (ec or $\beta^+ \rightarrow 0\%$, $\alpha \rightarrow 100\%$)

^{219}Rn (ec or $\beta^+ \rightarrow 0\%$, $\alpha \rightarrow 100\%$)

In Figure 9., a heatmap of the reaction is illustrated.

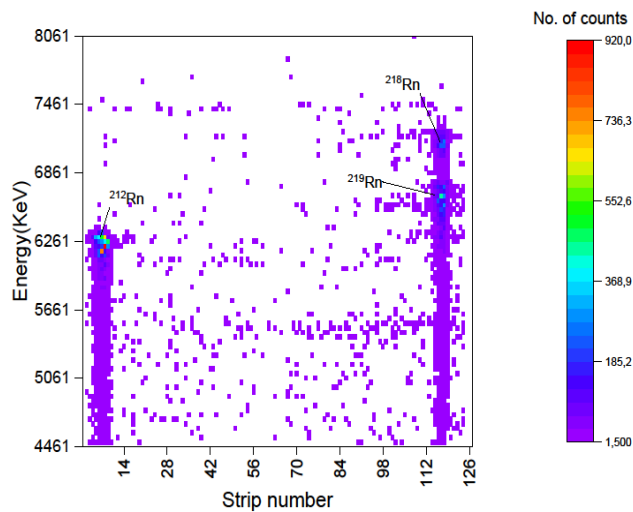


Figure 9. Heatmap of $^{48}\text{Ca} + ^{242}\text{Pu}$ reaction

5-Conclusions

The accuracy of the MASHA was confirmed by the calculation of the error, as the predicted values of the peaks in energy were confirmed. Analysis of the data, and further calibration of the energies revealed the energy spectra of the different isotopes. Further research is needed to perform these experiments for the fusion of heavier elements, requiring higher energies for the beam projectile and further upgrades to the target. The synthesis of flerovium was confirmed in the reaction of ^{48}Ca with ^{242}Pu by investigating its decay products, and also an estimate of its life time and mass could be determined. Progress in these experiments could provide eventual evidence for the existence of the so called “Island of stability”, which would be a great step forward in nuclear research.

6-Acknowledgments

I would like to thank the Joint Institute of Nuclear Research for granting me the opportunity to work in this project from which I could learn a lot, also I would like to thank my supervisor Mr Viacheslav Vedenev for his support in the project.

7-References

[1] S. N. Dmitriev, Y. T. Oganessyan, V. K. Utyonkov, S. V. Shishkin, A. V. Yeremin, Y. V. Lobanov, Y. S.

Tsyganov, V. I. Chepygin, E. A. Sokol, G. K. Vostokin, et al., “Chemical identification of dubnium as a

decay product of element 115 produced in the reaction $48\text{Ca} + 243\text{Am}$,” *Mendeleev Communications*, vol. 15,

no. 1, pp. 1–4, 2005.

[2] R. Eichler, N. Aksenov, A. Belozerov, G. Bozhikov, V. Chepigin, S. Dmitriev, R. Dressler, H. Gäggeler,

V. Gorshkov, F. Haenssler, et al., “Chemical characterization of element 112,” *Nature*, vol. 447, no. 7140,

pp. 72–75, 2007.

[3] V. Y. Vedenev, A. Rodin, L. Krupa, A. Belozerov, E. Chernysheva, S. Dmitriev, A. Gulyaev, A. Gulyaeva,

D. Kamas, J. Kliman, et al., “The current status of the masha setup,” *Hyperfine Interactions*, vol. 238, no. 1,

p. 19, 2017.

[4] A. Rodin, A. Belozerov, D. Vanin, V. Y. Vedeneyev, A. Gulyaev, A. Gulyaeva, S. Dmitriev, M. Itkis, J. Kliman,

N. Kondratiev, et al., “Masha separator on the heavy ion beam for determining masses and nuclear

physical properties of isotopes of heavy and superheavy elements,” *Instruments and Experimental Techniques*,

vol. 57, no. 4, pp. 386–393, 2014.